2004

Parallel molecular dynamics simulations of antimicrobial peptides

Svetlana V. Oard
Louisiana State University and Agricultural and Mechanical College, soard@agctr.lsu.edu

PARALLEL MOLECULAR DYNAMICS SIMULATIONS OF ANTIMICROBIAL PEPTIDES

A Thesis

Submitted to the Graduate Faculty of the
Louisiana State University and
College of Basic Sciences
in partial fulfillment of the
requirements for the degree of
Master of Science in Systems Science

in

The Department of Computer Science

by
Svetlana Oard
B.S., Melitopol State Institute of Education, 1986
Ph.D., Botany Institute of National Academy of Sciences of Ukraine, 1993
May 2004

ACKNOWLEDGEMENTS

I would like to express sincere appreciation to my advisor, Dr. Bijaya Karki, for support and encouragement in my research at Louisiana State University. I am grateful to Dr. Sitharama Iyengar for teaching me and serving as a chair on my committee. I am thankful to Dr. John Tyler for serving on my committee and to Dr. Aiichiro Nakano for helping to me at the beginning of my research.

Special thanks to my colleague, Satyavani Vemparala, as she was directly guiding me through my research. I am thankful to Dr. Brian D. Ropers-Huilman for providing the opportunity to use SuperHelix for the scaling tests.

Finally, I wish to express my gratitude to my dear family for supporting me throughout years of study.

TABLE OF CONTENTS

ABSTRACT

Molecular dynamics (MD) simulations of the wheat antimicrobial peptide β-purothionin were carried out in explicit water (~14,000 atoms) using an all-atom model. The structural properties of the peptide as a function of MD simulation, temperature, and presence of the mono- and divalent metal ions were investigated. The accuracy and scalability tests of the code Peach 3.8 for our system were performed on the Intel Xeon-based Linux cluster SuperHelix at Louisiana State University (LSU). The code showed the reliable accuracy and the parallel efficiency of 0.61 for ~14,000 particles on 16 processors. The microcanonical (MC) MD simulation of β-purothionin in water showed that all secondary structures were stable and exhibited normal conformation at 300 K initial temperature. Helicity of the peptide was found to depend strongly on temperature, consistent with experimental data. Analysis of the MD trajectories elucidated new details of temperature effects on purothionin. Thus, the α-helix α1 displayed unusual temperature resistance. The β-sheets and all four disulphide bonds were not affected by change in the range of temperature from 0 to 400 K. The residues Tyr13 and Arg30 thought to be involved in antimicrobial activity of purothionin displayed increased stability. Decrease in flexibility of the peptide largely decreased upon interaction with K^+ and Mg^{2+} ions. The MD simulations indicated that Mg^{2+} ions impaired the α-helix α2 and both ions interacted with Tyr13 and Agr30, suggesting the mechanism of cation inhibition for antimicrobial activity of purothionin. Therefore, the results reported here showed that the MC MD simulations reproduced effects of temperature and metal ions on structure of purothionin. Moreover, this study provided new insights into structural properties, and effects of temperature and metal ions on structure stability and conformation of the purothionin molecule.

CHAPTER 1

INTRODUCTION

Antimicrobial peptides are now recognized as an important component of non-specific host defense systems and innate immunity in insects, amphibians, plants, and mammals (Hancock and Lehrer 1998; Dathe and Wieprecht 1999). They are diverse in structure and characterized by a broad range of activity against bacteria, fungi, viruses and protozoa with disruption of membrane integrity (Niidome et al. 1999). Emergence of resistance against antimicrobial peptides is shown to be less probable than observed for conventional antibiotics (Zasloff 2002). These characteristics make antimicrobial peptides attractive targets for developing new antimicrobial compounds.

Plant antimicrobial peptides such as thionins display a broad spectrum of antibacterial and antifungal activity (Thevissen *et al.* 1996; Garcia-Olmedo *et al.* 1998). They are characterized as cysteine-rich, highly basic, 40 – 60 amino acids long peptides, arranged in a stem and arm configuration. Due to the presence of several basic amino acid residues, thionins are positively charged at neutral pH. This characteristic explains the charge-based interaction of a peptide with the membrane which is negatively charged. According to the Shai-Matsuzaki-Huanf model, the mechanism of action of most antimicrobial peptides is based on charge-based interaction followed by displacement of lipids, alteration of membrane structure, and entry of the peptide into the membrane and later the interior of the cell (Matsuzaki et al. 1999; Yang et al. 2000; Shai et al.1999). Experimental data suggest that the β-purothionin inserts into the hydrophobic core of the lipid bilayer upon interaction of residue Tyr13 with phospholipids (Richard et al. 2002). It significantly modifies the lipid packaging at the surface of the bilayer increasing the accessibility of water molecules. Moreover, data suggest that β-purothionin

generates cation-selective ion channels in cell membranes and artificial lipid bilayers (Hughes et al. 2000). Mono- and divalent metal ions interfere with the interaction of thionins and other antimicrobial peptides with phospholipid vesicles. Thus, 2-5 mM Ca^{2+} completely blocked activity of thionin, though 50 mM concentrations of monovalent ions like Na^{+} and K^{+} were necessary for inactivation (Hughes et al. 2000). Additional results indicated that increasing ionic strength reduced antimicrobial activity of most peptides including thionins (Thevissen et al. 1999; Zasloff 2002). However, the mechanism of cation inhibition of membrane disrupting activity of thionins is not known.

β-Purothionin is a natural antimicrobial peptide from the endosperm of wheat seeds. The three-dimensional structure of purothionins has been solved by NMR spectroscopy (Clore et al. 1987) and by X-ray diffraction (Rao et al. 1995; Stec et al. 1995). The tertiary structure of β-purothionin is a key to an important property, the disruption of membrane integrity in the wide range of cells. Investigation of the important β-purothionin properties is an area of great interest to reveal its mechanism of action and develop strategies for applications in developing effective antimicrobial compounds. To date, effects of temperature and interactions with mono- and divalent cations on purothionin structure and stability have not been studied in detail.

Molecular dynamics (MD) simulations have been used over the last 15 years to study the structure of various biomolecules. Recent advances in the computing resources and improvements in accuracy of force fields used to describe biological macromolecules have allowed the reproduction of experimental results in MD simulations (Aliste et al. 2003; Bathelt et al. 2002). These advances have created the possibility of direct comparison of MD calculations with experimental data of the same scale. Therefore, application of MD simulation analysis for refinement of experimental data and even replacing experiments with predictions has become

conceivable. Current available experimental results on the antimicrobial peptide β-purothionin provide a good starting point for further MD investigations.

The availability of software for MD simulations of large biomolecules with efficient scalability is an issue in improving computing performance in MD simulations with large size and time scales. We investigated the performance of the Peach ("Program for Energetic Analysis of bioCHemical molecules") software package for the MD simulation of biological molecules (Nemoto et al. 2002; Komeiji and Uebayasi 2002). It is a versatile collection of programs and libraries similar to conventional program packages such as Amber (Wang et al. 2000). Peach comprises several program modules where data are transmitted via intermediate files. The program modules are categorized into three segments: preprocessors which prepare input files for simulation, a simulator performing energy minimization and MD simulation, and a postprocessor analyzing the output files of the simulation (Komeiji et al. 1997). The parallelization of the code was performed by modifying the subroutines for the non-bonded interactions to allow use of the MPI library (Komeiji et al. 2001). The MD simulations of several important biological molecules were implemented using this software. All the simulations were conducted in an explicit solvent and the system size ranged from 10,000 to 40,000 particles. Results of 1 nsec MD simulations for Hin/hixL complex (Komeiji and Uebayasi 1999), *trp*-Repressor/Operator complex (Suenaga et al. 2000), and calmodulin, with or without Ca^{2+} (Komeiji et al. 2002) reproduced experimental data. The MD simulation of a pheromone binding protein performed with Peach 3.0 displayed flexibility of a loop supporting the hypothesis that the loop is a flexible lid (Nemoto et al., 2002).

MD simulations of proteins and other biomolecules require handling of large-scale systems (10^6 – 10^9 atoms). Significant progress has been made in parallelization of MD

simulations of biomolecules (Karplus and McCammon 2002; Tew et al. 2002). Strategies based on atom, force, and hybrid force/spatial decomposition were applied to develop parallel MD algorithms (Brooks et al. 1983; van Gunsteren and Berendsen 1988; Plimpton 1995). Earlier parallel MD algorithms were based on atom decomposition. The most advanced is the spatial or domain decomposition where a spatial domain is distributed uniformly among processors and particles can move across different processors. The most time consuming aspect of MD simulations of biomolecules consists of computing non-bonded forces (van der Waals (VDW) and Coulomb). Direct calculations of non-bond forces require $O(N^2)$ operations. Implementation of cutoff for VDW forces with algorithm using linked-cell neighbor lists reduces complexity to $O(N)$ (Yang et al. 1993). The particle mesh Ewald method reduces calculations of Coulomb forces to $O(N\log N)$ operations (Darden et al. 1993).

MD studies with Peach code were performed on the Grape-Peach system where Grape stands for "GRAvity piPE," a family of special hardware for N-body problems. Grape-Peach system is a specially designed high-performance simulator of biological molecules. However, analysis of Peach code performance on multipurpose parallel computers was not reported. Performance study of the code on the multipurpose parallel supercomputers is much needed to evaluate scalability and limits for a simulation system size and time scales.

The main objectives of this study were to analyze stability of β-purothionin in MD simulation at ambient temperature, temperature dependence of peptide structure, changes of the peptide structure in presence of mono- and divalent metal ions, and reproducibility of experimental data by a MC MD simulation. To address these questions performance of the Peach 3.8 code was tested on Intel Xeon-based Linux cluster SuperHelix. The all-atom force field Amber99 and MD simulation in explicit water (~14,000 atoms) were utilized to study

purothionin. K^+ and Mg^{2+} were utilized as the metal cations. A closely related area of interest is the dynamics of fluctuations at equilibrium of the molecules. Since these fluctuations may be of mportance for β-purothionin activity, we also performed the structure fluctuation analysis on a 125-psec time scale.

CHAPTER 2

SIMULATION METHODOLOGY

In molecular dynamics (MD) simulations, a physical system is represented by a set of N atoms and described as a trajectory which consists of positions $\{\mathbf{R}_i \mid i=1,\ldots,N\}$, and velocities, $\{\boldsymbol{V}_i \mid i=1,\ldots,N\}$ for all atoms. The trajectory is calculated using the Peach 3.8 code (Komeiji and Uebayasi 2002) by integrating the Newton's equations of motion,

$$m_i \frac{\partial^2 \mathbf{R}_i}{\partial t^2} = -m_i \sum_{j \neq i}^{N} \frac{m_j}{R_{ij}^3} \left(\mathbf{R}_i - \mathbf{R}_j \right) \tag{1}$$

where $\mathbf{R}_{i(j)}$ and $m_{i(j)}$ are the position vector and mass of atom *i(j)*.

The Newton's equations of motion are integrated using the velocity Verlet algorithm (Swope et al. 1982). The interatomic potential energy, U, encodes interactions among atoms and the essential component of MD simulations.

2.1 Interatomic Potential Model

A force field model (Komeiji et al. 1997) in which the interatomic potential energy consists of the bonded and non-bonded terms was used,

$$U = U_{bonded} + U_{non\text{-}bonded} \, . \tag{2}$$

U_{bonded} consists of bond, angle, and torsion interactions

$$U_{bonded} = U_{bond} + U_{angle} + U_{torsion} = \tag{3}$$

$$= \sum_{bonds} K_r \left(\mathbf{R} - \mathbf{R}_0 \right)^2 + \sum_{angles} K_\theta \left(\boldsymbol{\theta} - \boldsymbol{\theta}_0 \right)^2 + \sum_{torsions} \frac{V_n}{2} \left[1 + \cos\left(n\phi - \phi_0 \right) \right] \, ,$$

$U_{non\text{-}bonded}$ consists of VDW, 1-4 nonbonded, electrostatic, and 1-4 electrostatic interactions

$$U_{non\text{-}bonded} = U_{VDW} + U_{1\text{-}4VDW} + U_{Elc} + U_{1\text{-}4Elc} = \tag{4}$$

$$\sum_{i>j} \left[\left(\frac{a_{ij}}{R_{ij}} \right)^{12} - \left(\frac{b_{ij}}{R_{ij}} \right)^{6} \right] + \left(\frac{1}{SC_{14VDW}} \right) \sum_{1-4\,pairs} \left[\left(\frac{a_{ij}}{R_{ij}} \right)^{12} - \left(\frac{b_{ij}}{R_{ij}} \right)^{6} \right] + \sum_{i>j} \frac{q_i q_j}{R_{ij}} + \left(\frac{1}{SC_{14Elc}} \right) \sum_{1-4\,pairs} \frac{q_i q_j}{R_{ij}} \, ,$$

where K_r, $\mathbf{R}_0$, K_θ, $\boldsymbol{\theta}_0$, V_n, $\boldsymbol{\varphi}_0$, a_{ij}, b_{ij}, $q_{(i,j)}$, SC_{14Elc}, SC_{14VDW} are the force field parameters.

Atomic parameters used to describe all atoms were taken from the Amber99 force field library (Wang 2000).The long-range non-bonded interactions were calculated with a 12/20 Å twin-range cutoff. The neighbor list was updated every 10 steps. All of the MD simulations were performed in the microcanonical ensemble (MC) with the truncated octahedron periodic boundary conditions.

2.2 Multiple-Time-Scale Molecular Dynamics

The bonded interactions vary more rapidly than the non-bonded interactions. Since a time step (Δt) should be smaller than the smallest time scale, the different Δt can be used for computation of bonded and non-bonded forces. The multiple-time-scale (MTS) method separates the fast (small time scale for bonded interactions) and slow (large time scale for non-bonded interactions) modes significantly reducing the number of computations. We used an MTS algorithm drRESPA (Tuckerman et al. 1992) which divides interactions into three subsets, soft (bonded), medium (non-bonded VDW and for *(i,j)*=1-4pairs), and hard range forces (electrostatic)

$$\mathbf{F} = \mathbf{F}_\mathrm{s} + \mathbf{F}_\mathrm{m} + \mathbf{F}_\mathrm{h} \quad . \tag{5}$$

The Newton's equations of motion are integrated using the velocity Verlet algorithm within the drRESPA scheme:

$$G(\Delta t) = \exp\left(\frac{\Delta t}{2}\frac{f_s}{m}\frac{\partial}{\partial v}\right)\cdot\left[\exp\left(\frac{\Delta t_m}{2}\frac{f_m}{m}\frac{\partial}{\partial v}\right)\cdot\left\{\exp\left(\frac{\Delta t_h}{2}\frac{f_h}{m}\frac{\partial}{\partial v}\right)\cdot\exp\left(\Delta t_h v\frac{\partial}{\partial r}\right)\cdot\exp\left(\frac{\Delta t_h}{2}\frac{f_h}{m}\frac{\partial}{\partial v}\right)\right\}^K \cdot\exp\left(\frac{\Delta t_m}{2}\frac{f_m}{m}\frac{\partial}{\partial v}\right)\right]^L\cdot\exp\left(\frac{\Delta t}{2}\frac{f_s}{m}\frac{\partial}{\partial v}\right), \tag{6}$$

where Δt_m and Δt_h are time steps for the medium and hard forces that satisfy $\Delta t = L\,\Delta t_m$ and $\Delta t_m = K\Delta t_h$ (Komeiji et al. 1997). Choice of the time steps depends on the force field parameters, the

system to simulate, and desirable accuracy of computations. We tested three sets of time-steps for the bonded and non-bonded interactions, respectively, for MTS method and compared results with a single-time-step (STS) method. The accuracy test was performed on a Linux cluster SuperHelix (Dual Intel Pentium IV Xeon CPU/2.0GHz) using the Peach 3.8 code compiled on Intel 6.0 compiler. We performed 500-step MC MD runs of the neutralized system with total ~14,000 particles and 300 K initial temperature. The time steps (Δt) of 0.5, 1.0, 2.0, and 4.0 fsec were tested for the STS method. For the MTS method, the time steps for hard forces of 2.0, 4.0, and 8.0 fsec were used with the time step scheme n steps for hard, n x 2 steps for medium and n x 2 x 4 steps for soft range forces. (Table 1).

Table 1. Performance of a single-time-step (STS) and multiple-time-scale (MTS) methods depending on a time step (Δt) and the integration method for 500-step MC MD simulation of β-purothionin solvated in explicit water (total 14,170 atoms) at 300 K initial temperature.

Δt (fsec)	Integration Method	CPU(s)/ step	CPU(s)/ fsec	CPU Usage for non-bond forces(%)	$RMSF_r$ of total energy (kcal/mol)
0.5	STS	1.024	2.048	97.83	1.2E-03 (0.05%)
1.0	STS	1.008	1.008	97.80	5.4E-03 (0.2%)
2.0	STS	1.024	0.512	97.78	2.9E-02 (0.9%)
2.0	MTS	1.336	0.668	89.09	5.5E-04 (0.02%)
4.0	MTS	1.329	0.332	88.82	1.5E-03 (0.15%)
8.0	MTS	1.331	0.166	88.73	4.4E-02 (4.4%)

The evaluation of the stability of the integration was performed by computing the relative root mean square fluctuation ($RMSF_r$) of the total energy (E_t) for the trajectory:

$$RMSF_r = \left| \frac{\left\langle \left\langle \left(E_t - \langle E_t \rangle \right)^2 \right\rangle \right\rangle^{1/2}}{\langle E_t \rangle} \right| \quad , \qquad (7)$$

where 〈 〉 is a time average (Komeiji et al. 1997).

When the STS method was used, the Δt of 2 fsec resulted in the best CPU time per fsec of the MD simulation. However, the accuracy of energy calculations was unacceptable with the $RMSF_r$ at ~1%. Reduction of the Δt resulted in improvement of the accuracy, but simulation time increased significantly. When the MTS method was applied, sufficient accuracy with average RMSF of total energy ~0.1% was achieved using the larger Δt of 4 fsec. Our data were consistent with the accuracy reported for this time step in previous studies (Komeiji et al. 1997). The CPU time used per step in this simulation was three-fold smaller than the CPU time in simulation using the STS method and the Δt of 1 fsec which produced same accuracy. The implementation of the MTS method in our system allowed a 12-fold decrease in the CPU time used to compute a fsec of the simulation.

2.3 Molecular Model

β-Purothionin is a natural antimicrobial peptide from the endosperm of wheat seeds containing 45 amino acid residues. The initial structure of β-purothionin from wheat seed was obtained from the X-ray structure of Stec et al. (1995), determined at1.7 Å and pH 5.9, PDB entry 1BHP. The molecular fragments that constitute the secondary structures of β-purothionin are shown in Figure1 and Figure 2. The molecule is divided into two parts, the stem which consists of two antiparallel α-helices, α1 and α2, and the arm which contains a coil in extended conformation, L2, and a short antiparallel β-sheet formed by two β-strands, β1 and β2. This

tertiary structure is stabilized by four disulfide bonds with two bonds connecting the stem and another two bonds connecting the arm (Fig. 2 B).

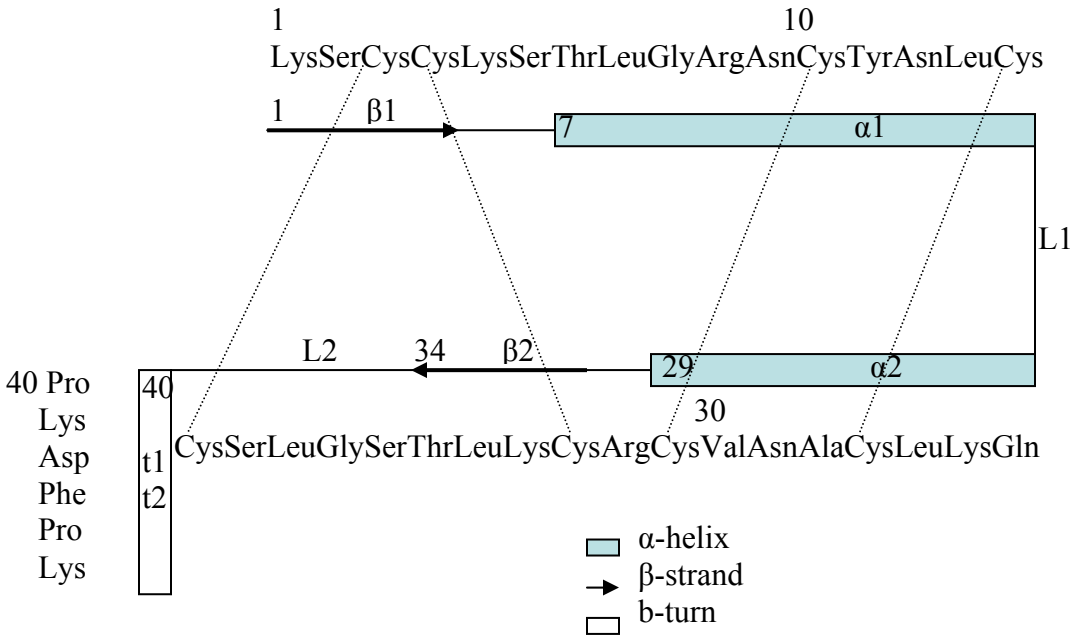

Fig.1. Amino acid sequence of β-purothionin. Secondary structural elements determined by X-ray crystallography (Stec et al. 1995) are labeled α for α-helix, β for β-strand, L for loop, t for b-turn. The disulfide bonds are shown by dashed lines.

All the crystallographically determined water and ligand molecules were removed. The coordinates of hydrogen atoms were then generated using the MKMOL function of Peach 3.8 (Komeiji and Uebayasi 2002) and minimized. Purothionin was solvated in an octahedral periodic boundary cell of TIP3P water. The width of the box was set to 12 Å from the border of the solvent-accessible surface. The chloride ions were added in amounts to neutralize the charged amino acids present in protein. The final solvated system consisted of one molecule of purothionin (685 atoms), 9 chloride ions, and 4,492 H_2O molecules resulting in 14,170 total atoms. The ions and water were then subjected to minimization using Steepest Dissent (SD)

method while holding all protein atoms rigid. Next, all atoms were allowed to move, and system was minimized for 100 steps using the SD method to relax any steric conflicts.

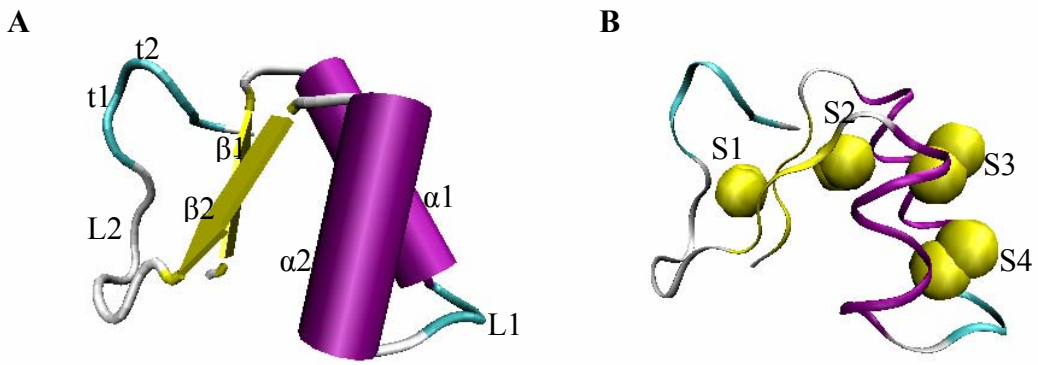

Fig. 2. Backbone model of the secondary structure of antimicrobial peptide, β-purothionin from wheat seed (X-ray structure). **A.** Structure representation with β-strands shown as yellow ribbons and α-helices as purple cylinders. **B.** Structure representation with four disulfide bonds shown as connected yellow spheres (two sulfur atoms), β-strands shown as yellow ribbons, and α-helices as purple ribbons.

Next, purothionin was simulated for 125 psec at 300 K initial temperature with the MTS method and the Δt of 4.0 fsec to study evolution of the molecular structure and stability in time. The temperature dependence of the structure stability was analyzed at 0, 100, 200, 300, 400 and 600 K initial temperatures with all other conditions kept the same as described above. Interaction of the peptide with metal ions was simulated at 300 K by adding 100 mM of K^+ ions or 20 mM Mg^{2+} ions for mono- and divalent metal ions, respectively, to the simulation box. The chloride ions were added in amounts to neutralize the added metal ions.

The conformational dynamics of the generated trajectories were analyzed by computing root mean square difference (RMSD) for main chain atoms, N, CA, and C atoms, and side chain atoms and root mean square fluctuation (RMSF). The RMSD between two structures *i* and *j* was calculated as follows:

$$RSMD = \left(1 \Big/ n \sum_{k-1}^{n} \left| \mathbf{R}_k^i - \mathbf{R}_k^j \right|^2 \right)^{1/2} \quad , \tag{8}$$

where $\boldsymbol{R}^i_k$ stands for the coordinate of the *k*-th main chain atom of structure *i*. The summation was performed over all *n* main chain atoms. The RMS Fluctuation around the time averaged structure was also computed for each amino acid residue to analyze the fluctuation pattern within the peptide. For visualization of structures and trajectories, the VMD1.8.1 was used (Humphrey et al. 1996).

2.4 Scalability Test

The Peach 3.8 code utilizes the MPI library for parallelization of MD computations (Komeiji et al. 2001). The parallelization of the code is based on force decomposition and performed by modifying the subroutines for the non-bonded interactions. The non-bonded interactions consist of VDW forces computed with cutoff and long-range Coulomb forces calculated using the particle mesh Ewald method (Darden et al. 1993). The cutoff for VDW forces is applied with the algorithm using linked-cell neighbor lists (Yang et al. 1993).

The test of computational scaling of the Peach 3.8 code for our system was performed on Intel Xeon-based Linux cluster SuperHelix at Louisiana State University. In SuperHelix 128 dual-processor nodes (Intel Pentium IV 2.0GHZ, 1024KB L2 cache, 3.2Gflop peak performance) are connected by Myrinet network with 100 MB Ethernet. The scalability tests were performed with 1-psec simulations at 300 K initial temperature, with STS method and time step of 1.0 fsec on 1, 2, 4, 8, 16, and 32 processors. Two system sizes were tested, with 14,170 and 35,240

atoms, where the latter system was prepared in the same manner as the former only with increased size of the simulation box and hence, increased number of water molecules. The parallel efficiency $\boldsymbol{S}$ was calculated as

$$\boldsymbol{S} = \boldsymbol{t_1} / \mathrm{P}\ \boldsymbol{t_P}\ , \qquad (9)$$

where t_P is the performance on P processors.

Because the number of atoms in our systems was fixed (N=14,170 and N=35,240), an increase in the number of processors used caused a proportional decrease in the number of atoms simulated per processor. For the smaller system (N=14,170), the MC MD simulation on one processor resulted in only 8.7 psec of the simulated time per day (Table 2).

Table 2. The scalability test for a system of β-purothionin solvated in explicit water with N=14,170 and N=35,240 atoms at 300 K initial temperature, STS method with Δt of 1 fsec.

Number of processor (P)	N=14,170			N=35,240		
	CPU(s)/fsec	Time Performance (ps/day)	Parallel Efficiency (%)	CPU(s)/fsec	Time Performance (ps/day)	Parallel Efficiency (%)
1	9.862	8.7	100	25.149	3.4	100
2	5.165	16.7	95.5	13.114	6.6	95.9
4	2.79	30.9	88.4	7.13	12.1	88.2
8	1.601	53.8	77.0	4.13	20.9	76.1
16	1.008	85.5	61.1	2.638	32.7	59.6
32	0.722	119.3	42.7	1.945	44.3	40.4

When the number of processors was increased to 32, the time performance increased 14-fold, though the parallel efficiency was only 43%. The parallel efficiency was 0.61 for ~14,000 particles on 16 processors with ~900 atoms per single processor and the simulation time performance of 85 psec per day. For the larger system (N=35,240), the parallel efficiency was very similar, and time performance decreased nearly 2.5-fold according to increase in the size of the system. For this system with N=35,240 and P=16 and N/P ~2000, the parallel efficiency was 0.6. Therefore, we did not observe system size dependence in the scalability of the code. The degradation of parallel efficiency for smaller N/P was caused by an increase of the ratio of communication time to computation time. Dependence of this ratio was reported previously on the MMD code for N/P of 5280, 10560, and 21120 particles, where parallel efficiency for 512 processors was ~80, 83, and 87%, respectively (Vemparala 2003). The proportional degradation of parallel efficiency was observed between tested N/P values with increase of P. Using SuperHelix, ~76% parallel efficiency was obtained on eight processors for N/P of 4405 atoms. However, the time performance was low in this case, only 21 psec per day (Table 2). The total execution time is another consideration for MD simulations of biomolecules since a time scale of MD simulations should approach a scale of biological processes $\geq$ 10 nsec. Choice of increase in time performance on terms of decrease in parallel efficiency may be necessary to achieve the biological time scale. Timing and parallel efficiency results were comparable with results shown for another parallel code for MD simulations of biomolecules, Gromacs 3.0 (Lindahl et al. 2001). Implementation of the MTS method with the Δt of 4 fsec on 16 processors tripled the time performance in comparison with the STS method as expected according to the data in Table 1, producing 263 psec of MC MD simulation time per day.

In summary, the best accuracy / CPU usage per step was achieved in the MC MD simulation of β-purothionin solvated in explicit water with the MTS integration method using the Δt of 4 fsec. The best parallel efficiency / time performance corresponded to 16 processors.

CHAPTER 3

RESULTS AND DISCUSSION

3.1 Structure Stability of β-Purothionin in the MC MD Simulation

To study the structural stability of purothionin in MD simulations, the 125-psec long MC MD simulation in explicit water with the number of atoms of 14,170 was performed at 300 K initial temperature using the MTS method and the Δt of 4 fsec. Averages and fluctuations of several energies were calculated for the 125-psec trajectory to examine stability of the peptide simulation (Fig. 3).

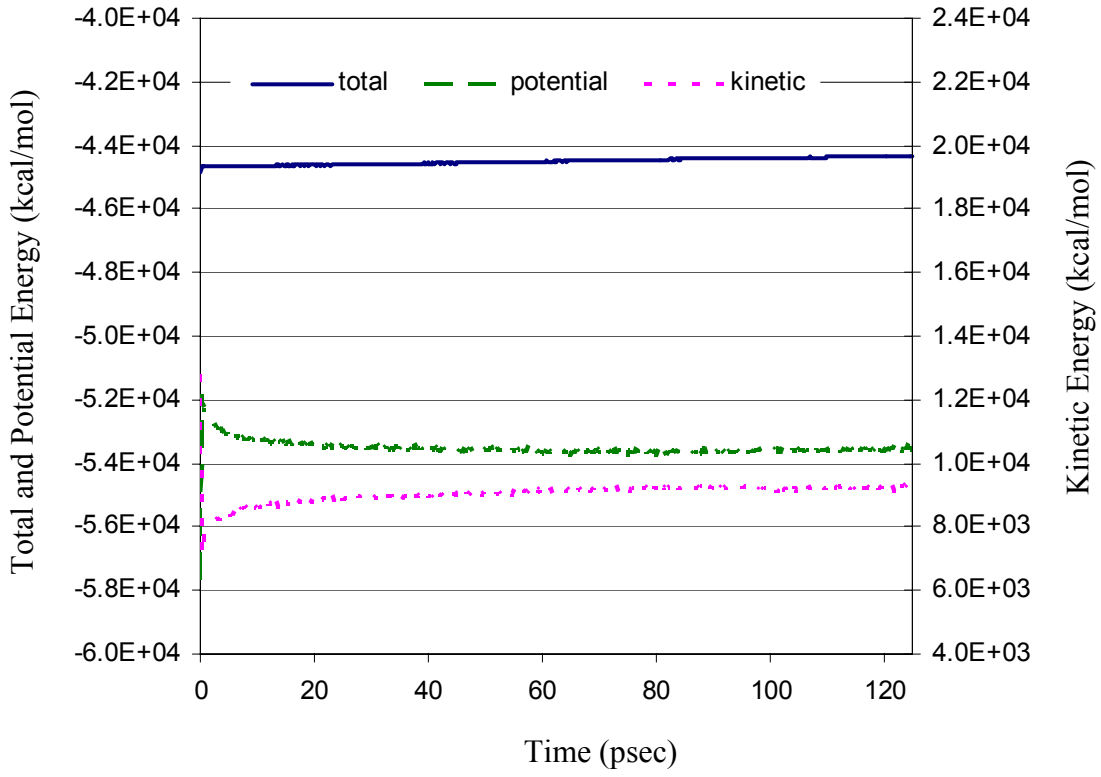

Fig. 3. Change of total, kinetic, and potential energies in MC MD simulation of purothionin at 300 K initial temperature.

The total energy fluctuation, $RMSF_r$, was as small as 0.2%. The kinetic and potential energies showed fluctuations 3.5 and 0.49%, respectively. Thus, the MC MD simulation trajectory was considered stable from an energetic viewpoint. All secondary structures and disulphide bonds were intact after 125-psec of simulation (Fig. 4 A, B). Superposition of the initial and MD structure showed structural stability of the peptide during the MD simulation since all secondary structures and disulphide bonds showed nearly identical configurations (Fig. 4 C, D). The time evolution of the root mean square deviation (RMSD) of the MD trajectory from the X-ray structure was computed to analyze a structure stability of β-purothionin (Fig. 5 A). The RMSD increased rapidly to 0.8 Å for the main and 1.5 Å for the side chain atoms, respectively, within the first 2 psec of the simulation. Then, the RMSD values gradually decreased for the main and increased for side chain atoms. The total RMSD values were less than 1.3 Å indicating high structural stability of purothionin. Additional confirmation of stability was shown by decrease of the RMSD for the main chain atoms over the simulation time. Together, the total energy fluctuation and time evolution of the RMSD values showed that the chosen set of simulation parameters was adequate for MD simulation of purothionin.

The effectiveness of the MS simulation was verified by reproducing the protein structure and dynamics obtained from experimental data. Analysis of the RMSD and root mean square fluctuation (RMSF) around the time average structure for each residue showed that this simulation reproduced characteristics of residues found by the MNR and CD spectra experiments (Vila-Perello et al., 2003). Analysis of the RMSD showed that Leu15, Arg19, Gln22, Lys23, Arg30, and Leu37 deviated the most from the initial structure with side chain RMSD ranging from 1.8 to 3.0 Å (Fig. 5 A). These results fit well with characteristics of amino acids in an aqueous solution. Thus, an increase in RMSD for Leu15 and Leu37, which are aliphatic

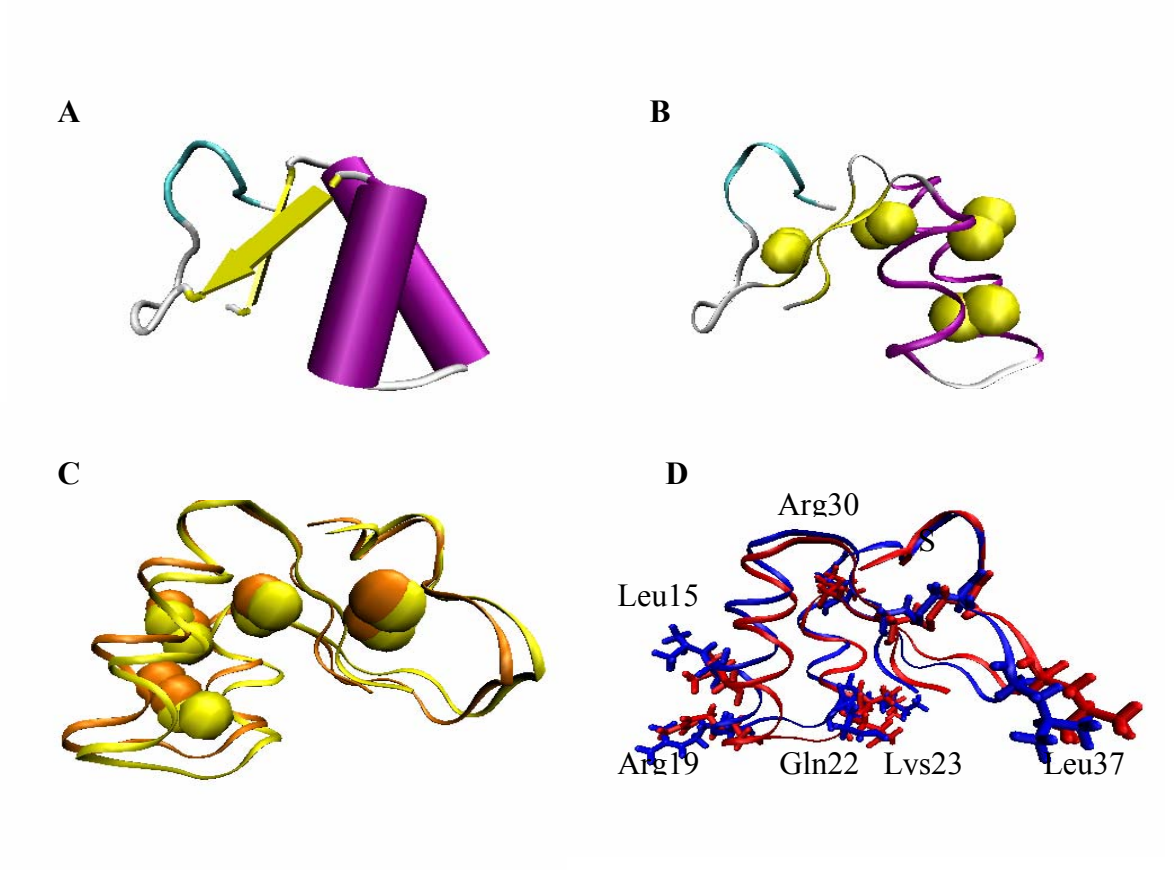

Fig. 4. Backbone model of the secondary structure of β-purothionin after 125-psec long MC MD simulation at 300 K initial temperature. **A,** Structure representation with β-strands shown as yellow ribbons and α-helices as purple cylinders. **B,** Structure representation with four disulfide bonds shown as connected yellow spheres (two sulfur atoms), β-strands shown as yellow ribbons, and α-helices as purple ribbons. **C,** Superposition of the MC MD trajectory produced at 300 K with the crystal structure shown in orange and yellow, respectively. **D,** Structure representation for superposition of the MC MD trajectory produced at 300 K with the crystal structure shown in red and blue respectively. Backbones are shown as ribbons, the side chains of most affected residues are shown as licorices and labeled. S – the side chains of Cys3 and Cys39 forming the disulfide bond are shown as licorices.

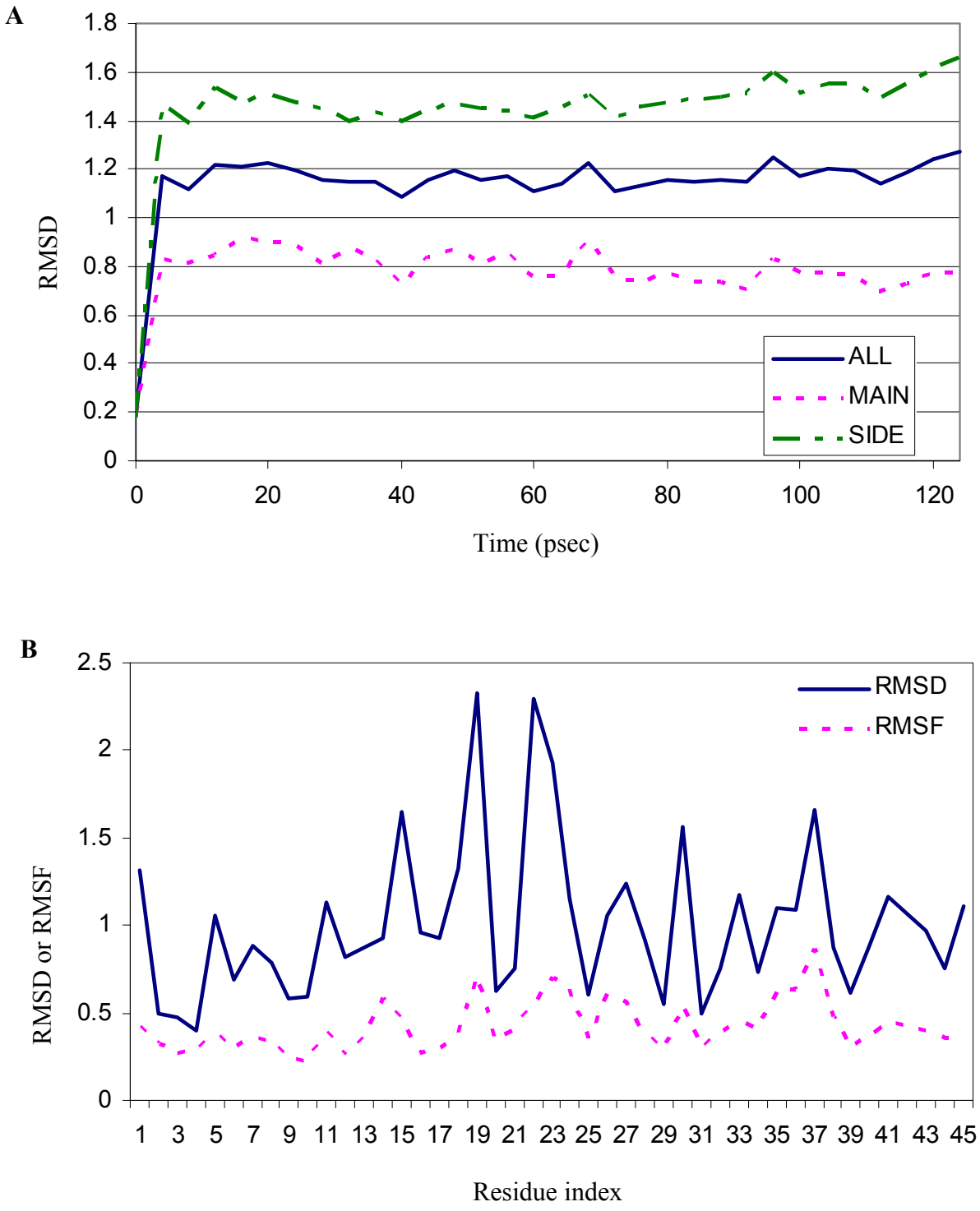

Fig. 5. MC MD simulation of β-purothionin at the 300 K initial temperature. **A**, Time evolution of RMS Deviation between the MD & crystal structures. **B**, RMSD and RMSF as functions of the residue indices.

residues, was caused by repulsion upon their contact with water molecules. Arg19 is the charged residue at the top of the hairpin structure that makes it flexible. Results of our simulation confirmed this since Arg19 showed the largest RMSD. Arg30 was located between two secondary structures and charged. Gln22 and Lys23 were both positively charged immediate neighbors and, therefore, experienced mutual repulsion. In contrast, all 8 Cys residues were among the most stable residues with side chain RMSD $\leq$ 1.0 Å in our simulation. They formed 4 disulfide bonds which significantly restricted movement.

The RMSF pattern showed that Arg19, Lys23, Leu24, Ser35, Gly36, and Leu37 fluctuated the most during the MD simulation (Fig. 5 B). Comparison of the RMSD and RMSF for each residue elucidated the details of structural dynamics of β-purothionin in water. β-purothionin is amphipathic like the majority of antimicrobial peptides. It has the hydrophobic residues on the outer surface and hydrophilic residues on the inner surface of both helices. The hydrophilic residue, Arg30, is also located on the outer surface of the corner between the stem and arm (Rao et al. 1995; Stec et al. 1995). The MD trajectory displayed that Leu15, which is hydrophobic, underwent directed movement upon repulsive interaction with water molecules toward more hydrophobic peptide core created by two α-helices. Arg30 also displayed directed motions due to interaction with surrounding residues. Arg19 displayed mostly fluctuating motion since it is the charged residue positioned at the top of the loop L1 forming a hairpin structure in the peptide; hence it was mostly surrounded with water and did not interact with other residues. Ser35, Gly36, and Leu37 were located in a loop L2 where Leu37 was mostly surrounded with water molecules. The repulsive interaction of Leu37 with water molecules caused its own and the neighbor's fluctuating motions. These data were in good agreement with experiments showing that loops were more flexible than helices or strands (Nemoto et. al. 2002). The majority of

residues in the α-helix α1 and both β-sheets showed small fluctuating or directed motions and therefore, large structural stability. In contract, the majority of residues in the α-helix α showed fluctuating motions indicating lower structural stability of α2 in the aqueous solution in comparison with other secondary structures of β-purothionin. All Cys residues fluctuated the least, consistent with the presence of disulfide bridges that restrict mobility. Interestingly, Tyr13, which is conserved among thionins and thought to play a major role in the toxicity (Fracki et. al. 1992), exhibited small RMSD and RMSF values. Our simulation showed that the α-helix α1 which contains Tyr13 in the middle was more stable than α2 at 300 K. Thus, the MC MD simulation of β-purothionin solvated in explicit water showed that all secondary structures of the peptide were stable and exhibited normal conformation at 300 K initial temperature.

3.2 Temperature Dependence of the Peptide Structure

Temperature dependence of purothionin structure stability was analyzed in the 125-psec MC MD simulations at 0, 100, 200, 300, 400 and 600 K initial temperatures. Averages and fluctuations of several energies and temperature for each MD simulation are listed in Table 3. Values for the total and potential energies gradually decreased with increase of temperature from 0 to 600 K. The $RMSF_r$ values increased for total and potential energies with increase of the initial temperature. The $RMSF_r$ showed that the simulation trajectories at the starting temperatures from 0 to 400 K were energetically stable (Nemoto et al., 2002) since total and potential energy fluctuations were ≤ than 0.5%. The MC MD simulation with 600 K initial temperature was considered energetically unstable since the total energy fluctuated 2.5 %, suggesting instability of the whole system at this temperature.

Table 3. Averages and fluctuations of energies of β-purothionin in 125-psec MC MD simulations at different temperatures.

Temperature (K)		Total Energy	Potentia Energy	Kinetic Energy
Initial	Average ±RSMF	± $RMSF_r$ (kcal/mol)	± $RMSF_r$ (kcal/mol)	± $RMSF_r$ (kcal/mol)
0	63±5	-57500±8.6E-04 (0.1%)	-60180±2.0 E-03	2676±7.6E-02
100	119±6	-53090±1.9E-03 (0.2%)	-58120±3.3E-03	5027±5.4E-02
200	169±7	-48860±1.6E-03 (0.2%)	-56010±4.2E-03	7155±4.0E-02
300	214±7	-44500±2.3E-03 (0.2%)	-53530±4.9E-03	9030±3.5E-02
400	250±8	-40020±5.1E-03 (0.5%)	-50550±6.2E-03	10540±3.0E-02
600	326±13	-30520±2.5E-02 (2.5%)	-44270± 1.6E-02	13750± 4.0E-02

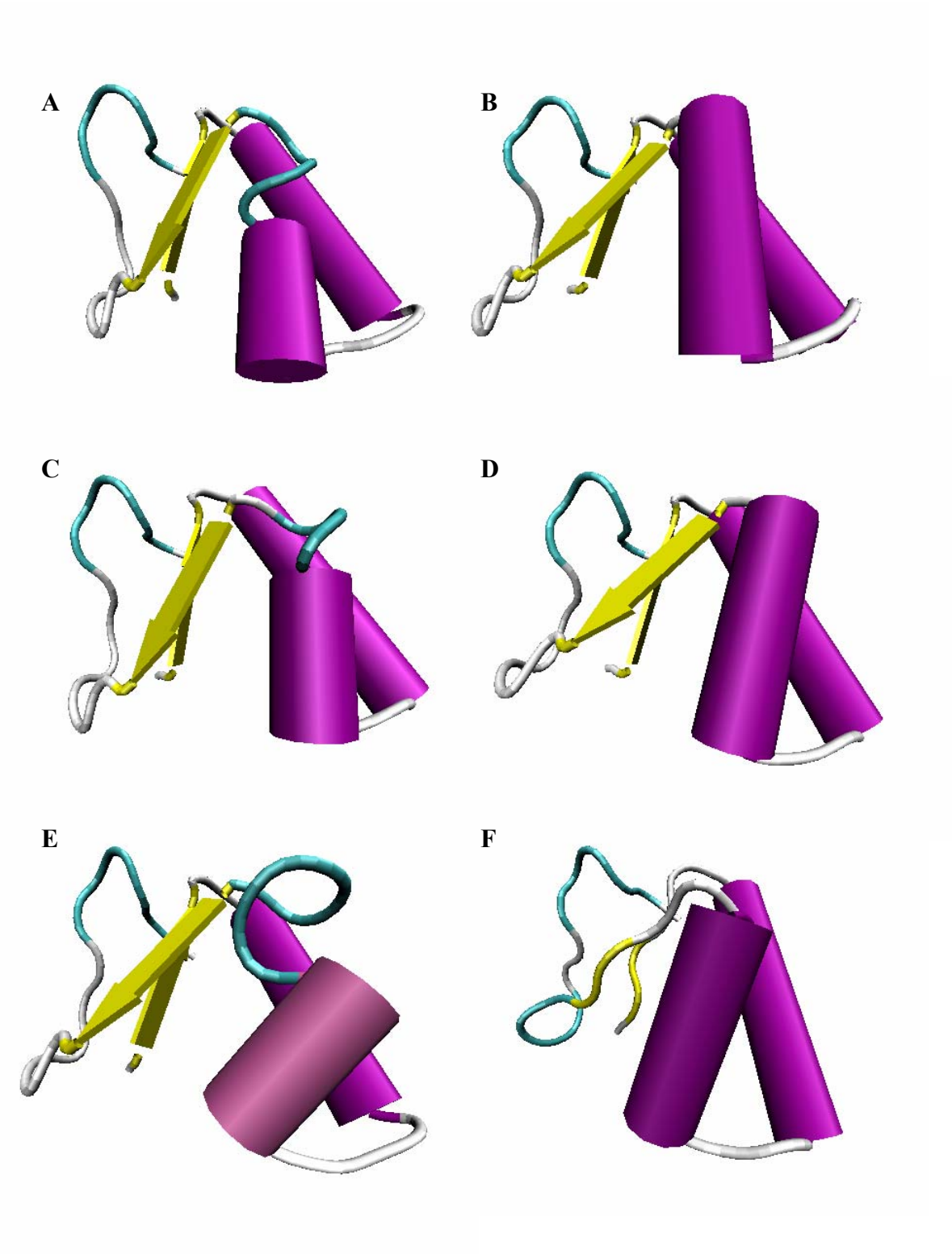

Fig. 6. Effect of temperature on the secondary structure of β-purothionin. Structure representation with β-strands shown as yellow ribbons, α-helices as purple cylinders, loops as white and b-turns as blue tubes. Backbone models of MD trajectories for **A**, 0, **B**, 100, **C**, 200, **D**, 300, **E**, 400, and **F**, 600 K initial temperature.

Comparison of secondary structures for the MD trajectories at various temperatures indicated that the peptide was stable during MD runs only at 100 and 300 K (Fig. 6 B, D). The MD structure at 300 K initial temperature corresponded the best to the crystal one as not only all secondary structures were preserved, but the tilt between α-helices and β-sheets was similar as well (Fig. 2, 6 D). The structural stability of the purothionin trajectories from MC MD simulations at 0, 200, 400, and 600 K was impaired. It is interesting to note that the α-helix α1 was stable at all temperatures tested. High thermal stability of a α-helix was also observed in a bacterial TrwC protein which could withstand heating without unfolding at 90 degrees C for 10 min (Arrondo et al. 2003). Stability of α-helix α2 and both β-sheets varied with change of temperature. The α-helix α2 showed the least stability and was affected at both, low and high temperatures displaying the pattern "unstable – stable – unstable – stable - unstable – stable" with sequential change of temperature from 0 to 600 K. Thermal denaturation experiments showed the helical pattern of purothionin to be fully preserved between 5 and 80 °C (Vila-Perello et al., 2003) which is consistent with our results since both helices were preserved in the MD simulation at 300 K. The β-sheets were affected only at the highest temperature tested (Fig. 6 F) supporting experimental data of higher stability of β-sheets in comparison with α-helices (Perczel et al. 2003; Berisio et al. 2002).

The time evolution of RMSD of MD structures from the crystal structure was computed to analyze effect of low and high temperatures on the structure stability of β-purothionin (Fig. 7). The RMSD values of the peptide structure simulated at 0 and 100 K were the largest, however, that did not fluctuate significantly over the simulation time. Moreover, the RMSD values for 100 K slightly gradually declined confirming the overall stability of the structure. The MD trajectory at 200 and 300 K were next in stability with RMSD values smaller than for 100 K showing

smaller changes from the initial structure. However, they displayed an increase in RMSD fluctuation over the time in comparison with the MD structures at 0 and 100 K. The time evolution of RMSD at high temperatures displayed growth on structural instability where RMSD was continuously increasing for 400 K or greatly fluctuating for 600 K trajectories, respectively. Our results fit well with experimental data where the purothionin structure was stable in a range from 5 to 80 C (Vila-Perello et al. 2003). In general, higher temperatures than ambient are more detrimental to a protein structure than lower temperatures (Smeller 2002; Xu et al. 2003). Therefore, the MC MD simulation of temperature dependence of β-purothionin structure successfully reproduced experimental data.

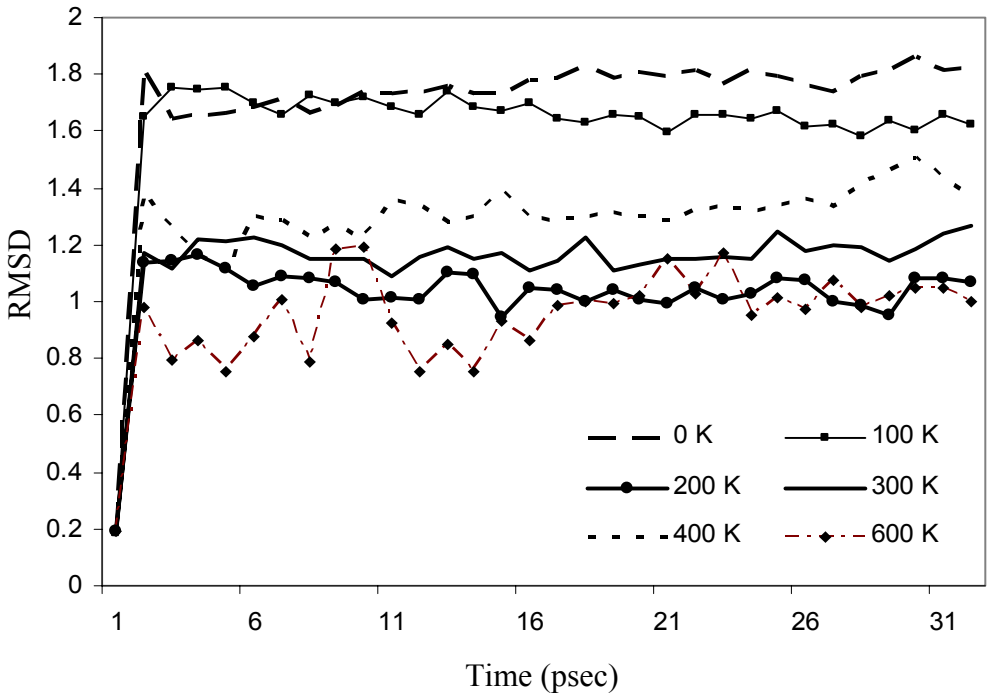

Fig. 7. Time evolution of RMS Deviation between the MD & crystal structures at different temperatures.

Analysis of the RMSD and RMSF values for each residue at different temperatures provided detailed information on the contribution of each residue to stability of secondary

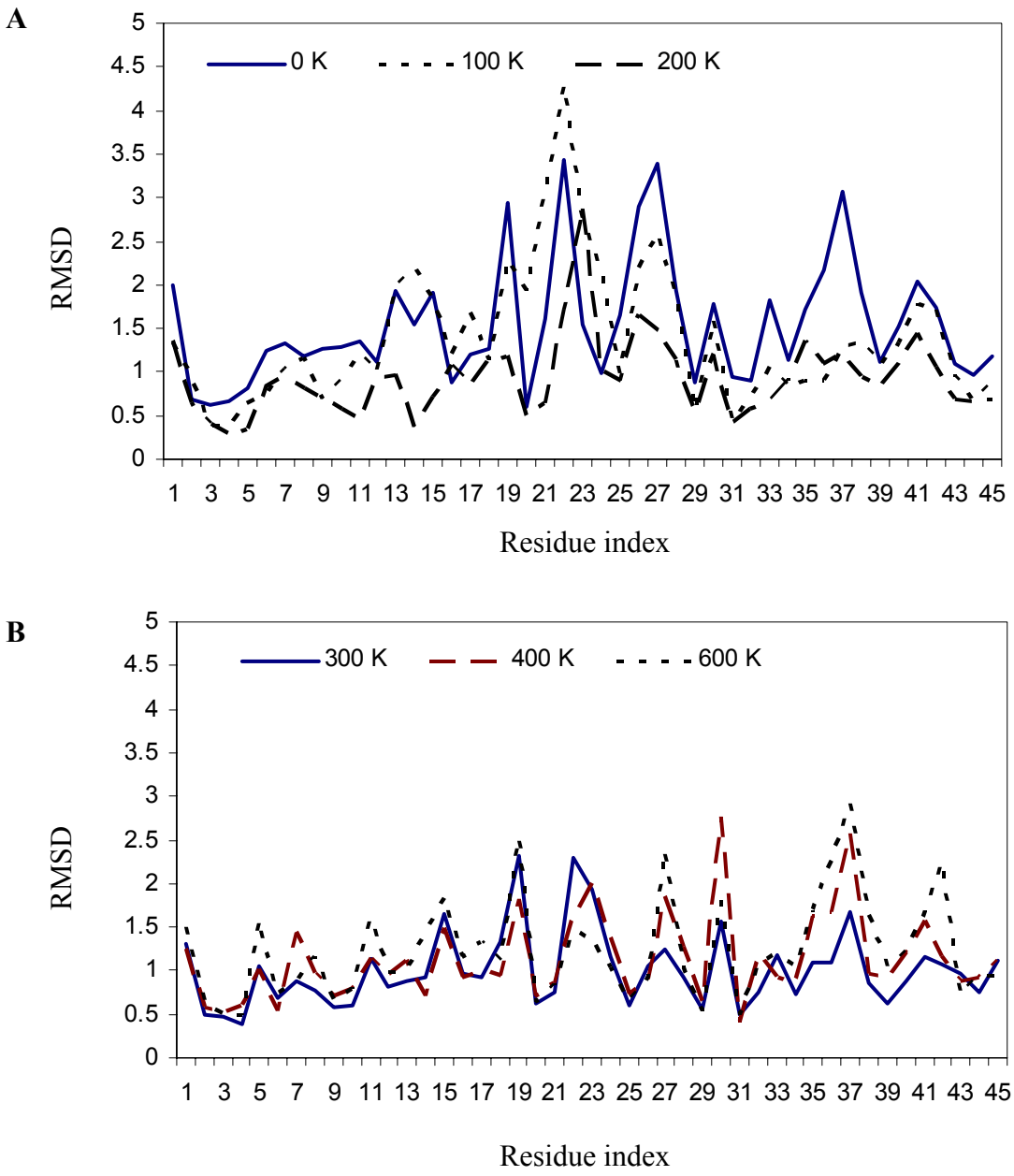

Fig. 8. RMS Deviation between crystal and MD structures as function of the temperature and residue indices. **A**, RMSD at low temperatures. **B**, RMSD at ambient and high temperatures.

structures in purothionin (Fig 8, 9). All residues of β-sheets showed small RSMD and RMSF

values at all temperatures, except at 600 K. The small values of RSMD were observed for all

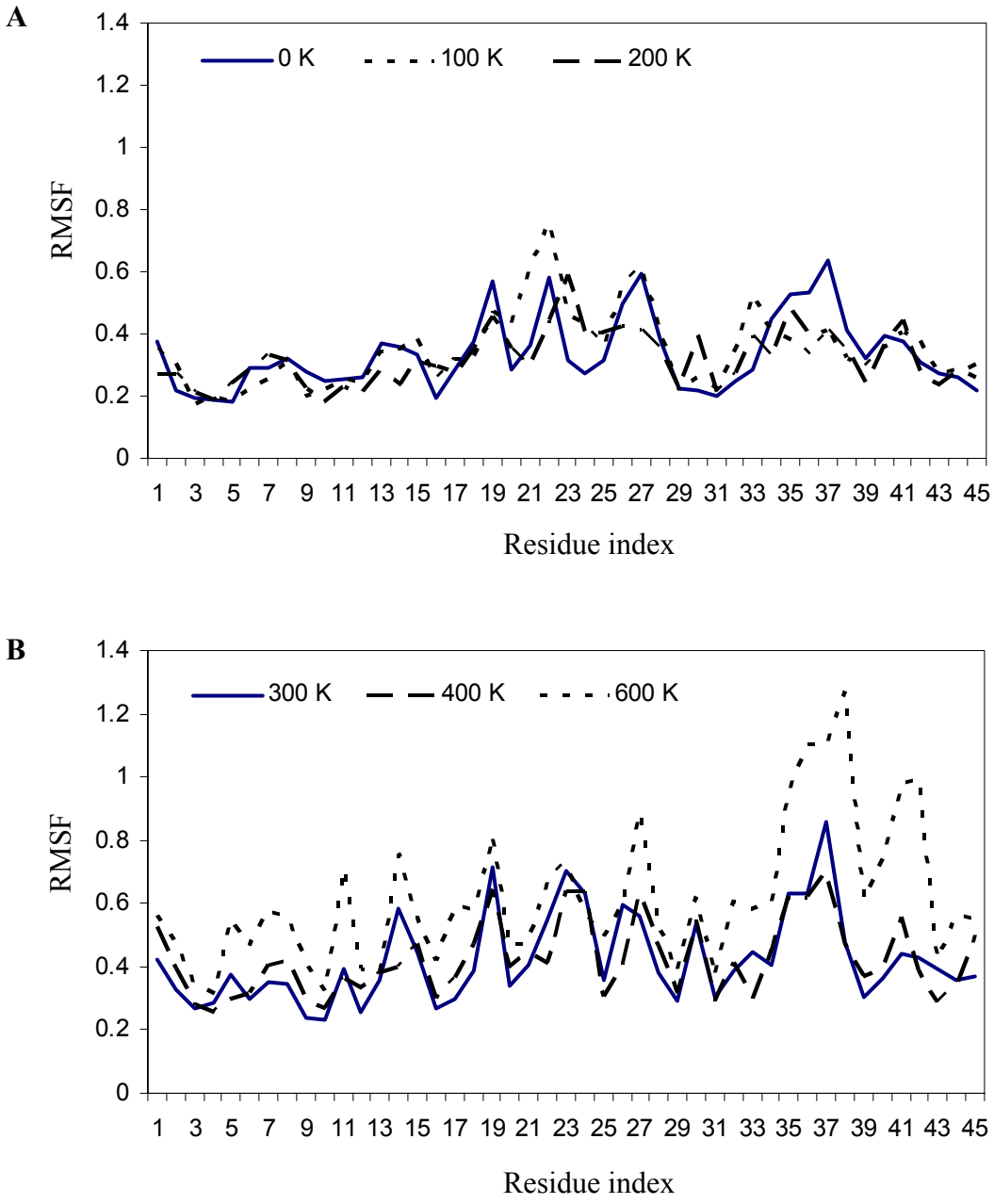

Fig. 9. Effect of temperature on RMS Fluctuation around the time averaged structure as function of residue indices . **A**, RMSF at low temperatures. **B**, RMSF at ambient and high temperatures.

residues of the α-helix α1 at low temperatures even though the RMSF values indicated fluctuating motions at its C-end.

The RSMD and RMSF values for the residues of the loop L1 and α-helix α2 greatly varied at low temperatures indicating large instability of this secondary structure. Gln22 and Asp27 were the residues contributing the most to instability of the α2. Both loops largely fluctuated at all temperatures, however, the large changes in RMSD were observed only at 0, 400, and 600 K suggesting large shifts in the whole molecule.

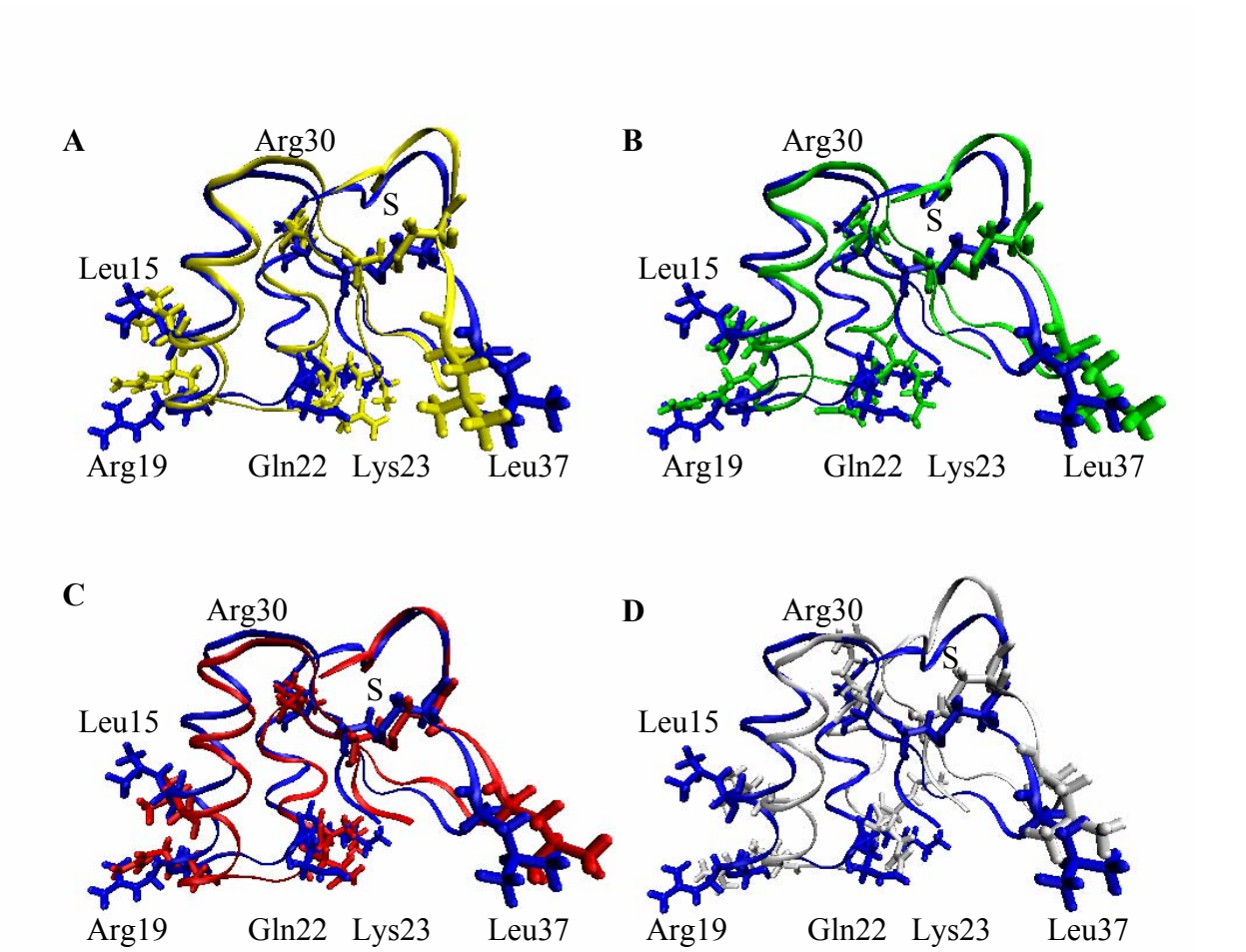

Fig. 10. Schematic diagram of β-purothionin crystal structure superposed on the MC MD trajectory produced at temperatures of **A -** 0, **B** – 100, **C** – 300, and **D** – 400 K. The crystal structure is colored in blue. Backbones are shown as ribbons, the side chains of most affected residues are shown as licorices and labeled. S – the side chains of Cys3 and Cys39 forming the disulfide bond are shown as licorices.

All four disulphide bonds were not affected by change of temperature in the tested range since Cys residues were relatively rigid at all tested temperatures with main chain RMSD ≤ 0.6 Å. The RMSD for Agr30 was similar for all temperatures, except for 600 K where it increased two-fold. This residue was located between two disulphide bonds formed by Cys4-Cys31 and Cys12-Cys29 (see Fig. 1) largely restricting the amplitude of its motion. Arg30 can be used to monitor strength of these bonds. Similarity in RMSD values for Arg30 in the range of temperatures between 0 and 400 K confirmed absence of changes in these two disulphide bonds and therefore, large temperature resistance. Tyr13 which is thought to be important for antimicrobial activity of purothionin (Fracki et al. 1992; Hughes et al. 2000) did not significantly change conformation at all temperatures suggesting unusual conformational stability. Interestingly, the MD trajectory at elevated temperature 400 K was energetically stable and displayed accurately changes in the peptide structure upon heating. These results are similar with reported previously MD simulations at 400 K which were successfully used for ab initio fast folding simulations of small proteins (Jang et al. 2003).

Therefore, the MC MD simulations at different temperatures provided confirmation of experimental data about temperature stability of purothionin. In addition these simulations displayed details on temperature effects for each secondary structure of purothionin. Thus, we found that all disulphide bonds and β-sheets are highly temperature resistant contributing to overall temperature resistance. Among α-helices, the α-helix α1 is unusually stable and supports very conserved conformation of Tyr13. The α-helix α2 is the least temperature resistant secondary structure in purothionin suggesting large flexibility of this part of the peptide. These results are informative for future applications in particular application of the sequence of unusually stable α-helix.

3.3 Effect of Mono- and Divalent Metal Ions

Two molecular dynamics simulations were performed to simulate K^+ and Mg^{2+}-dependent conformational changes of β-purothionin. Concentrations of metal ions used in the simulations were chosen to fully inhibit antimicrobial activity of purothionin according to experimental data, 100 and 20 mM for K^+ and Mg^{2+}, respectively (Vila-Perello et al. 2003; Richard et al. 2002, Zasloff 2002). The MC MD simulations of the peptide in presence of both metal ions were energetically stable (data not shown).

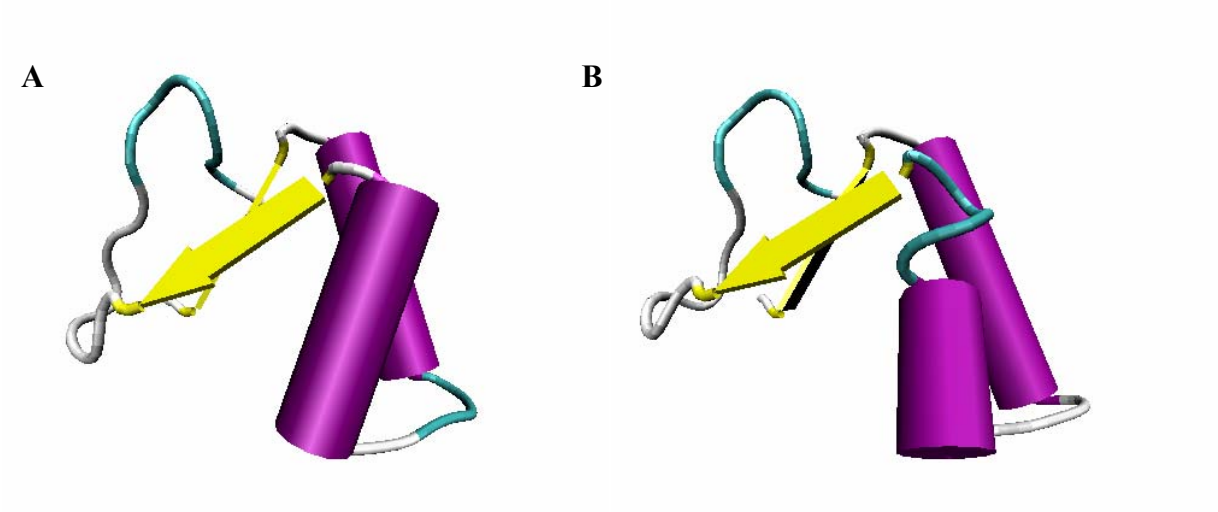

Fig. 11. Backbone model of the secondary structure in presence of the monovalent and divalent metal ions: **A,** 100 mM K^+ and **B,** 20 mM Mg^{2+}. Structure representations with β-sheets shown is yellow,α-helices as purple ribbons, and b-turns as blue tubes.

All secondary structures of the peptide were maintained in presence of K^+ ions (Fig. 11 A). Analysis of the MC MD trajectory of purothionin with Mg^{2+} ions displayed the large conformational changes upon presence of the divalent ions in the α-helix α 2 and in the loop L1 (Fig. 11 B). The secondary structures of the α-helix α 1 and both β-sheets were present.

Time-dependent changes of the RMSD from the initial crystal structure of the peptide in presence of K^+ ions were larger than with no ions (Fig. 12). Addition of Mg^{2+} ions resulted in

doubled increase in the differences between the RMSD with and without ions in comparison with K^+ ions. The RMSD values fluctuated less over 125 psec of the MD simulation in presence of monovalent cations than with divalent cations or without cations suggesting decrease of structural flexibility of the peptide. The gradual decrease of RMSD for the MD trajectories with both metal ions was observed over 125 psec of the MD simulation. These data strongly suggested increase of the structural stability in presence of metal cations.

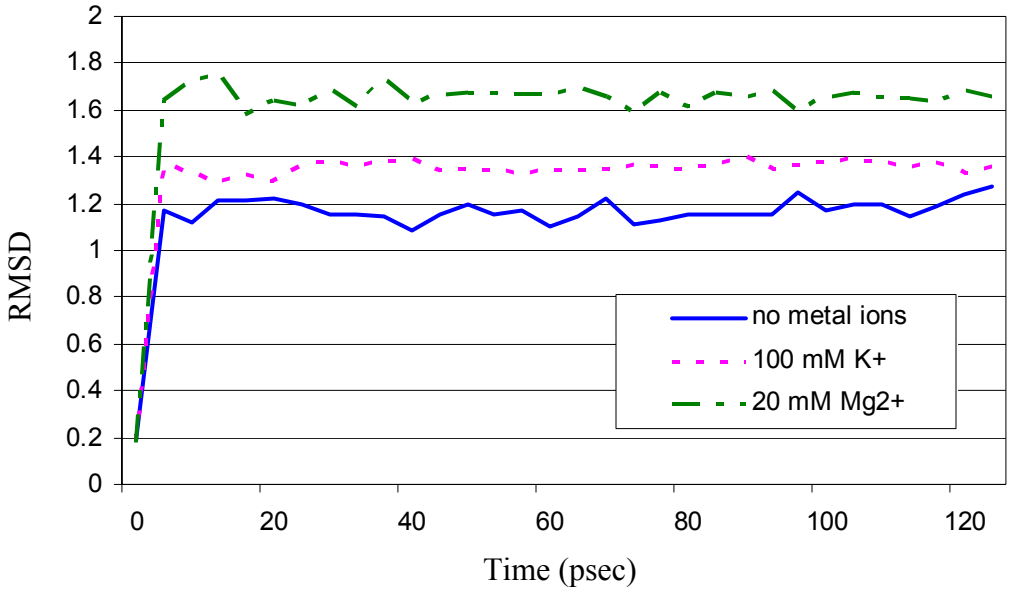

Fig. 12. Time evolution of RMS Deviation between MD and crystal structures of purothionin in presence of the monovalent and divalent metal ions, K^+ and Mg^{2+}.

Comparison of the RMSD and RMSF for each residue between the MD trajectories with mono- and divalent ions showed ion dependent variation in a pool of affected amino acid residues. Thus, K^+ interacted with the C-end of α-helix α2, loop L2, and both b-turns as indicated by increase of their RMSD values in comparison with no ions added (Fig. 13). Interestingly, the RMSF values were significantly smaller for all residues indicating a significant decrease in the peptide flexibility similarly to data for the time evolution of RMSD values. The RMSF values indicated larger decrease in the peptide flexibility in presence of K^+ than Mg^{2+} ions. However,

several secondary structures such as α-helix α2 and loop L1 were impaired by interaction with Mg^{2+} as indicated by changes in RMSD values between the initial and MD structures (Fig. 13).

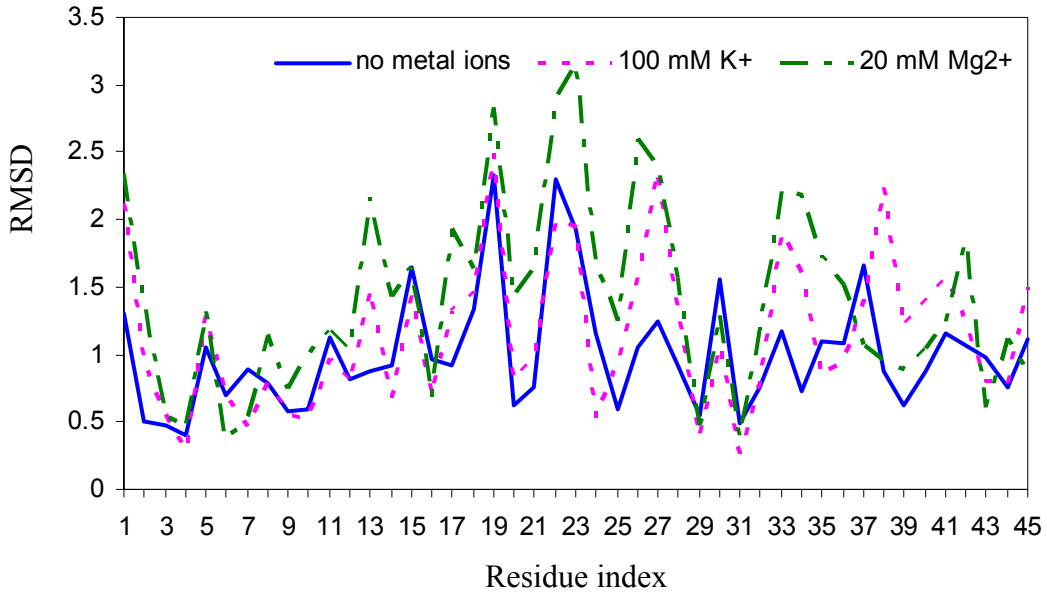

Fig. 13. RMSD between MD and crystal structures as function of the residue indices in presence of the monovalent and divalent metal ions, K^+ and Mg^{2+}.

We observed similar RMSD for Arg30 in all three MD structures; however, RMSF values were three-fold smaller in presence of both ions suggesting interaction of both cations with this residue. Another similarity between mono- and divalent cations was observed in the increase of RMSD values for all residues of the β-sheet β2. Interestingly, our data displayed the interaction of both ions with Tyr13 with Mg^{2+} ions interacting stronger than K^+. In addition the RMSF values decreased two – to three fold in response of the peptide on presence of metal cations (Fig. 14).

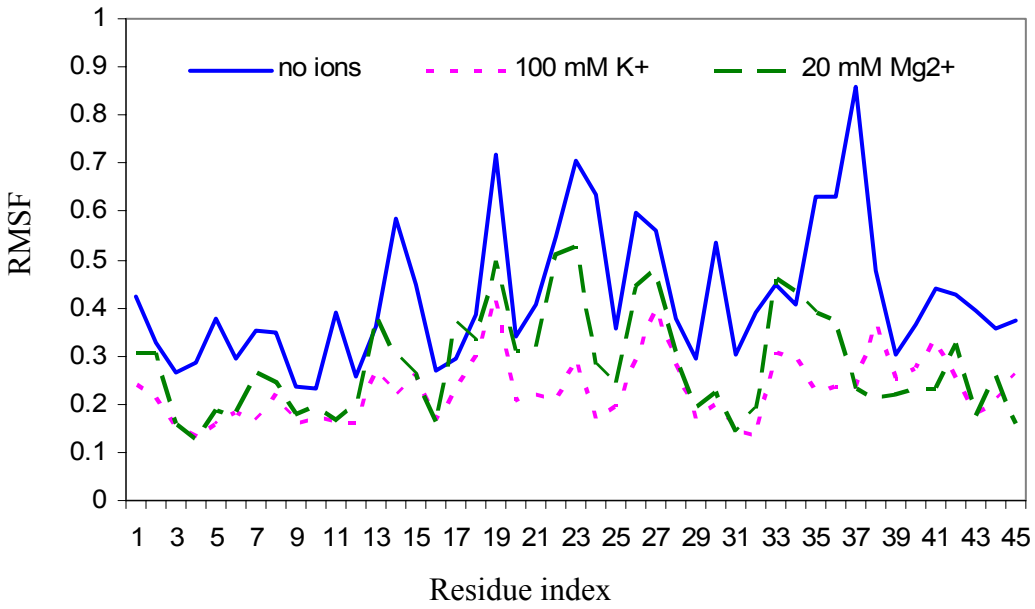

Fig. 14. RMS Fluctuation around the time averaged structure as function of the residue indices in presence of the monovalent and divalent metal ions, K^{+} and Mg^{2+}.

These results reproduced characteristics of purothionin found by the MNR and CD spectra (Hughes et al. 2000). Both the experimental data and our MD simulations suggested that cations increase the rigidity of purothionin causing loss of antimicrobial and membrane permeabilizing activity (Hughes et al. 2000; Richard et al. 2002). The MD simulation with metal ions revealed that cations interact with both important for the activity residues, Tyr13 and Arg30 that evidently contributes to inactivation of purothionin.

3.4 Conclusions

Molecular dynamics (MD) simulations of the antimicrobial peptide β-purothionin from wheat seed was carried out in explicit water (~14,000 atoms) using an all-atom model. The structural properties of the peptide as a function of MD simulation, temperature, and presence of the mono- and divalent metal ions were investigated. The MD simulations were performed in a periodic boundary using microcanonical (MC) ensemble. To perform simulations reported in this study, the accuracy test of Peach 3.8 code was completed on our system and accurate computations were obtained with a multiple time step integrator and time step of 4 fsec. The scalability test of the code for our system was performed on Intel Xeon-based Linux cluster SuperHelix at LSU. The code showed the parallel efficiency of 0.61 for ~14,000 particles on 16 IBM processors. The scalability did not depend on the size of the system. The timing and parallel efficiency results were comparable with results shown for another parallel code for MD simulations of biomolecules, Gromacs 3.0 (Lindahl et al. 2001).

The MC MD simulation of β-purothionin fully solvated in water showed that all secondary structures of the peptide were stable and exhibited normal conformation at 300 K initial temperature. Helicity of the peptide was found to depend strongly on temperature. The α-helix α2 contributed primarily to the observed temperature dependence, while α1 displayed unusual temperature resistance for both decrease and increase of temperature. This observation was consistent with experimental results of temperature effects on helicity of purothionin where helicity was shown to be consistent between 5 and 80 °C. The β-sheets and all four disulphide bonds were not affected by change in the range of temperature from 0 to 400 K. These data suggest that disulphide bonds mainly contribute to high temperature resistance of purothionin. The MD simulations demonstrated new important details of purothionin structure, playing

apparently the main role in antimicrobial properties. Thus, analysis of MD trajectories displayed increased stability of the residues thought to be involved in antimicrobial activity of purothionin, Tyr13 and Arg30.

Finally, MD simulations were performed to simulate the metal ion-dependent conformational changes of purothionin. The simulations of K^+ and Mg^{2+} bonded forms of purothionin were completed in solution starting from the X-ray structure. Concentrations of metal ions were set to fully inhibit antimicrobial activity of purothionin according to experimental data, 100 and 20 mM for K^+ and Mg^{2+}, respectively. The large differences were observed between the trajectories with and without metal ions. The flexibility of the peptide largely decreased upon interaction with both K^+ and Mg^{2+} ions. These results were in agreement with experimental data. The MD simulation results indicated that both ions interacted with Tyr13 and Agr30. These results were not reported before and suggest that the inhibition of purothionin activity by metal ions is caused by competitive interaction of the ions with Tyr13 and Arg30, reducing or blocking completely their interactions with microbial membranes.

Therefore, the reported here results showed that the MC MD simulations reproduced experimental data about effects of temperature and metal ions on structure of purothionin. Moreover, the MD simulations provided new insights about structural properties, and effects of temperature and metal ions on structure stability and conformation of purothionin. The unusual stability of the α-helix α2 detected in this study requires further investigation to determine the characteristics determining helical stability. This information has potential application for engineering thermally stable proteins. In addition, our results validate the accuracy of the MD computations and reliability of *in silico* mutagenesis study to substitute experiments on mutagenesis.

REFERENCES

Aliste, M., MacCallum, J. and Tieleman, D. (2003) Molecular dynamics simulations of pentapeptides at interfases: salt bridge and cation - π interactions. *Biochemistry* **42,** 8976-87.

Arrondo, J., Echabe, I., Iloro, I., Hernando, M., de la Cruz, F. and Goni, F. M. (2003) A bacterial TrwC relaxase domain contains a thermally stable alpha-helical core. *J Bacteriol* **185,** 4226-32.

Bathelt, C., Schmid, R. and Pleiss, J. (2002) Regioselectivity of CYP2B6: homology modeling, molecular dynamics simulation, docking. *J Mol Model* **8,** 327-35.

Berisio, R., Vitagliano, L., Mazzarella, L. and Zagari, A. (2002) Recent progress on collagen triple helix structure, stability and assembly. *Protein Pept Lett* **9,** 107-16.

Brooks, B., Bruccoleri, R., Olafson, B., States, D., Swaminathan, S. and Karplus, M. (1983) CHARMM: A program for macromolecular energy, minimization and dynamics calculations. *J Comp Chem* **4,** 187-217.

Clore, G., Sukumaran, D., Gronenborn, A., Teeter, M., Whitlow, M. and Jones, B. (1987) Nuclear magnetic resonance study of the solution structure of a1-purothionin. *J Mol Biol* **193,** 571-78.

Darden, T., D. York., and L. Pedersen (1993) Particle mesh Ewald: an N.log(N) method for Ewald sums in large systems. *J Chem Phys* **98,** 10089-92.

Dathe, M., Wieprecht, T. (1999) Structural features of helical antimicrobial peptides: their potential to modulate activity on model membranes and biological cells. *Biochimica et Biophysica Acta* **1462,** 71-87.

Fracki, W., Li. D., Owen, N., Perry, C., Naisbitt, G. and Vernon, L. (1992) Role of Tyr and Trp in membrane responses of Pyrularia thionin determined by optical and NMR spectra following Tyr iodination and Trp modification. *Toxicon* **30,** 1427-40.

Garcia-Olmedo, F., Molina, A., Alamillo, J.M. and Rodriguez-Palenzuela, P. (1998) Plant defense peptides. *Biopolymers* **47,** 479-91.

Hancock, R. a. L., R. (1998) Cationic peptides: a new source of antibiotics. *Trends in Biotechnology* **16,** 82-88.

Hughes, P., Dennis, E., Whitecross, M., Llewellyn, D. and Gage, P. (2000) The cytotoxic plant protein, b-purothionin, forms ion channels in lipid membranes. *Journal of Biological Chemistry* **275,** 823-927.

Humphrey, W., Dalke, A and Schulten, K. (1996) VMD – Visual Molecular Dynamics. *J Molec Graphics* **14,** 33-38.

Jang, S., Kim, E., Shin, S. and Pak, Y. (2003) Ab initio folding of helix bundle proteins using molecular dynamics simulations. *J Am Chem Soc* **125,** 14841-6.

Karplus, M., McCammon, J. A. (2002) Molecular dynamics simulations of macromolecules: a perspective. *Nature Struct Biol* **9,** 646-52.

Komeiji, Y., Uebayasi, Y., Takata, R., Shimizu, A., Itsukashi, K. and Taiji, M. (1997) Fast and accurate molecular dynamics simulation of a protein using a special-purpose computer. *J Comput Chem* **18,** 1546-63.

Komeiji, Y., and Uebayasi, M. (1999) Change in conformation by DNA-peptide association: molecular dynamics of the Hin-recombinase-hixL complex. *Biophys J* **77,** 123-38.

Komeiji, Y. a. U., M. (2002) Peach-Grape system - a high performance simulator for biomolecules. *Chem-Bio Informatics Journal* **2,** 102-18.

Lindahl, E., Hess, B. and van der Spoel, D. (2001) GROMACS 3.0: a package for molecular simulation and trajectory analysis. *J Mol Model* **7,** 306-17.

Matsuzaki, K. (1999) Why and how are peptide-lipid interactions utilized for self-defence? Magainins and tachyplesins as archetypes. *Biochim Biophys Acta* **1462,** 1-10.

Nemoto, T., Uebayasi, M. and Komeiji, Y. (2002) Flexibility of a loop in a pheromone binding protein from *Bombyx mori*: a molecular dynamics simulation. *Chem-Bio Informatics Journal* **2,** 32-37.

Niidome, T., and Anzai, S. (1999) Effect of amino acid substitution in amphiphilic a-helical peptides on peptide-phospholipid membrane interaction. *Journal of Peptide Science* **5,** 298-305.

Perczel, A., Jakli, I., Csizmadia, I. (2003) Intrinsically stable secondary structure elements of proteins: a comprehensive study of folding units of proteins by computation and by analysis of data determined by X-ray crystallography. *Chemistry* **9,** 5332-42.

Plimpton, S. (1995) Fast Parallel algorithm for short range molecular dynamics. *J Comp Phys* **117,** 1-19.

Rao, U., Stec, B. and Teeter, M. (1995) Refinement of purothionins reveals solute particles important for latice formation and toxicity. 1. a1-purothionin revisited. *Acta Crystallogr, Sect D* **D51,** 904-13.

Richard, J.-A., Kelly, I., Marion, D., Pezolet, M. and Auger, M. (2002) Interaction between β-purothionin and dimyristoylphosphatidylglycerol: A ^{31}P-NMR and infrared spectroscopic study. *Biophys J* **83,** 2074-83.

Shai, Y. (1999) Mechanism of the binding, insertion and destabilization of phospholipid bilayer membranes by a-helical antimicrobial and cell non-selective membrane-lytic peptides. *BIochim Biophys Acta* **1462,** 55-70.

Smeller, L. (2002) Pressure-temperature phase diagrams of biomolecules. *Biochim Biophys Acta* **1595,** 11-29.

Stec, B., Rao, U., Teeter, M. M. (1995) Refinement of purothionins reveals solute particles important for lattice formation and toxicity. Part 2: Structure of beta-purothionin at 1.7 angstroms resolution. *Acta Crystallogr, Sect D* **51,** 914.

Suenaga, A., Yatsu, C., Komeiji, Y., Uebayasi, M., Meguro, T. and Yamato, I. (2000) Molecular dynamics simulation of *trp*-repressor/operator complex: analysis of hydrogen bond patterns of protein–DNA interaction. *J Mol Struct* **526,** 209-18.

Swope, W., Andersen, H., Behrens, P. and Wilson, K. (1982) A computer simulation method for the calculation of equilibrium constants for the formation of physical clusters of molecules: Application to small water clusters. *J Chem Phys* **76,** 637-49.

Tew, G., Liu, D., Chen, B., Doerksen, R., Kaplan, J., Carroll, P., Klein, M. and DeGrado, W. (2002) De novo design of biomimetic antimicrobial polymers. *Proc Nat'l Acad Sci USA* **99,** 5110-14.

Thevissen, K., Terras, F. and Broekaert, W.F. (1999) Permeability of fungal membranes by plant defensins inhibits fungal growth. *Applied Environmental Microbiology* **63,** 5451-58.

Tuckerman, M., Berne, B. and Martyna, G. (1992) Reversible multiple time scale molecular dynamics. *J Chem Phys* **97,** 1990-2001.

Vila-Perello, M., Sanchez-Vallet, A., Garcia-Olmedo, F., Molina, A. and Andreu, D. (2003) Synthetic and structural studies on Pyrularia pubera thionin: a single-residue mutation enhances activity against Gram-negative bacteria. *FEBS Letters* **536,** 215-19.

Vemparala, S. (2003) Scalable parallel molecular dynamics algorithms for organic systems. Thesis, Louisiana State University, 53 p.

Wang, J., Cieplak, P. and Kollman, P. A. (2000) How well does a restrained electrostatic potential (RESP) model perform in calculating conformational energies of organic and biological molecules? *J Comput Chem* **21,** 1049-74.

Xu, Y., Oyola, R. and Gai, F. (2003) Infrared study of the stability and folding kinetics of a 15-residue beta-hairpin. *J Am Chem Soc* **125,** 15388-94.

Yang, L., Brooks III, E. and Belak, J. (1993) A linked-cell domain decomposition method for molecular dynamics on a scalable multiprocessor. *Scientific Programming* **2,** 153-62.

Yang, L., Weiss, T., Lehrer, R. and Huang, H. (2000) Crystallization of antimicrobial pores in membranes: magaini and protegrin. *Biophys J* **79,** 2002-09.

Zasloff, M. (2002) Antimicrobial peptides of multicellular organisms. *Nature* **415,** 389-95.

VITA

Svetlana Oard was born in Melitopol, Ukraine. In 1986, Svetlana obtained her bachelor's degree with a major in biology and chemistry and minor in mathematics at Melotopol State Pedagogical Institute. In 1993, she earned her doctoral degree in cell biology from M. G. Kholodny Botany Institute of UAS, Kiev, Ukraine.

In 2000, Svetlana entered the master's program in the Department of Computer Sciences at Louisiana State University in Baton Rouge, Louisiana. She expects to graduate with the degree of Master of Science in Systems Science in Spring of 2004.